Dalton Transactions

Accepted Manuscript

ROYAL SOCIETY OF CHEMISTRY

www.rsc.org/dalton

Cite this: DOI: 10.1039/c0xx00000x

www.rsc.org/xxxxxx

ARTICLE TYPE

Citrate-hydrazine hydrogen-bonding driven single-step synthesis of tunable near-IR plasmonic, anisotropic silver nanocrystals: Implications in SERS spectroscopy of inorganic oxoanions†

Satarupa Pattanayak,[a] Abhishek Swarnakar[b], Amiya Priyam[c,#,*] and Gopal M. Bhalerao[d]

Received (in XXX, XXX) Xth XXXXXXXXX 20XX, Accepted Xth XXXXXXXXX 20XX
DOI: 10.1039/b000000x

A simplified, single-step aqueous synthesis route to tunable anisotropic silver nanocrystals (NCs) has been developed by tailoring the hydrogen-bonding interactions between a mild stabilizer, sodium citrate, and a mild reductant, hydrazine hydrate. The structure directing ability of the H-bonding interaction was harnessed by keeping a stoichiometric excess of hydrazine under ambient conditions (pH 7, 25 °C). Decreasing the synthesis temperature to 5 °C imparts rigidity to citrate-hydrazine H-bonding network, and the plasmon peak moves from 500 to 550 nm (using 40 mM hydrazine). On lowering the pH from 7 to 5, the H-bonding is further strengthened due to partial protonation of citrate and the plasmon peak is tuned to 790 nm. Further, we found that, at 5 °C and pH 5, there also exists a sub-stoichiometric regime in which the maximum tunability of plasmon peak (790→1010 nm) is achieved with 1 mM hydrazine. HR-TEM reveals that the near-IR plasmonic NCs are nanopyramids having pentagonal base with edge length varying from 15 nm to 30 nm. Through second derivative FTIR analysis, a correlation between hydrogen-bonded molecular vibrations and the plasmon tunability has been established. The anisotropic NCs exhibit significant Raman enhancement on the citrate molecules. Further, a solution-phase, non-resonant SERS spectroscopic detection method for an inorganic contaminant of ground water, arsenite, has also been developed.

1. Introduction

Anisotropic noble metal nanocrystals (NCs) have caught the imagination of scientists around the globe due to their interesting plasmonic, electrical, magnetic and catalytic properties[1]. Nanorods and oblate spheroids represent the simplest of these structures. Besides, complex geometrical shapes have also evolved over the years that include nanoprisms, nanoplates, nanodiscs, tetrahedron, decahedron, nanorice, nanobars etc.[2]. These nanomaterials show remarkable plasmon tunability from visible (Vis) to near-IR (NIR) region. Due to the robust plasmonic properties in the biologically transparent window (650-1200 nm), they are ideally suited for several biomedical applications such as darkfield imaging,[3] photothermal therapy[4], analytical sensors[5] etc. Recently, some innovative applications of these NCs in photovoltaics,[6] fuel cells[7] and catalysis[8] have also come up.

In contrast to anisotropic nanoparticles, spherical nanparticles exhibit very limited plasmon tunability with change in size. For example, on increasing the size of gold nanoparticles from 10 to 100 nm, the plasmon peak moves from 520 nm to 580 nm only.[9] This restricts their biomedical applications. However, by controlled aggregation or self-assembly of these spherical nanoparticles it is possible to tune the plasmon wavelength to the NIR region which is biologically transparent.[10] The redshift occurs due to plasmon-plasmon coupling that result from near-field interactions.[10b] Various morphologies such as dimers, linear nanochains and globular nanoassmeblies have been reported previously by controlling the surface chemistry of these nanoparticles. However, such NIR plasmonic assemblies may become very large in size measuring upto few micrometers.[10a] Further, the NIR plasmon band is too broad in these self-assembled structures. These considerations make them difficult to use for in-vitro or in-vivo applications. So, it is desirable to develop small, well-dispersed nano-sized anisotropic nanocrystals which have robust NIR plasmonic properties.

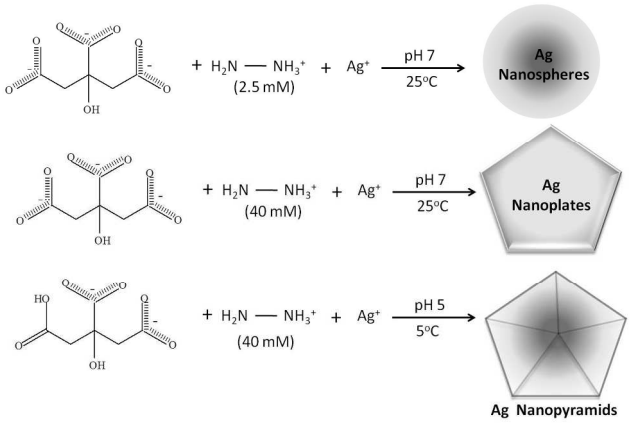

Scheme 1. An illustration of single-step synthesis scheme for Ag anisotropic NCs. H-bonding network between reductant and stabilizer undergoes a change with variation in temperature, pH and hydrazine concentration which directs the anisotropic growth of nanocrystals.

Several synthesis methodologies have been developed to obtain anisotropic plasmonic nanoparticles of a variety of shapes and sizes. However, most of them are multi-step processes involving preparation of seed nanocrystals which on further chemical treatment or light-irradiation grow into various

geometrical pattern.[11] Polyol synthesis is an alternative non-seed mediated approach, but the reagents are added in multiple steps over several hours. It also employs an additional structure directing agent such as CTAB or CTAC or PVP.[2c,12,13] Trace amount of certain inorganic species can further alter the shape of such nanocrystals.[2d]

In this work, we present a single step synthesis of anisotropic silver nanocrystals having shapes tunable from nanoplates to nanopyramids and having versatile tunability of plasmon peaks that spans visible to near-IR spectral region, 500-1010 nm. We use the simplest of reagents, hydrazine hydrate (reductant) and sodium citrate (stabilizer), to make plasmonic nanocrystals with complex geometrical features. Our approach of using 'mild-reductant, mild stabilizer' obviates the need for seeds or additional structure directing agents.

Although previous researchers[14] made attempts for one pot synthesis using citrate-hydrazine and $AgNO_3$ in water, it yielded micrometer-sized crystals of varying shapes without any plasmon tunability. Ghader et al[15a] synthesized truncated triangular silver nanoparticles (edge length: 94 nm) using similar reagent system and could get a limited plasmon tunability from 625 to 740 nm. In another work by Cao et al,[15b] EDTA was necessitated as shape directing agent in addition to citrate-hydrazine to prepare triangular and hexagonal silver nanoplates having Vis-to-NIR tunability of plasmon bands. This process was slow as it involved vigorous stirring of Ag_2O in water for one day and subsequent transfer of supernatant (dissolved Ag^+ ions) to another vessel. In contrast, our method yields much smaller anisotropic silver nanocrystals (edge length: 15-30 nm) having Vis-to-NIR tunability (500-1010 nm) in a single shot addition of reagents, citrate-hydrazine and $AgNO_3$, thus simplifying the whole synthesis process. Second derivative FTIR analysis implicates hydrogen bonding between citrate and hydrazine as the key factor responsible for versatile tunability of shape and plasmon band. These NCs show enhanced Raman scattering for citrate. Further, the application potential of the NCs in analyte detection is also underscored as strong SERS enhancement is obtained for arsenite ions**,** a common contaminant of ground water.

2.Experimental Section

2.1Materials:

Silver nitrate (99.5%), trisodium citrate (99%), hydrazine hydrate (80%), Sodium hydroxide (98%), . All the chemicals were purchased from Sigma Aldrich and were used as obtained.

2.2 Synthesis: Our simplified synthesis approach for anisotropic silver NCs is based on tuning the hydrogen bonding interaction between reductant and stabilizer and using its directional character to promote anisotropic crystal growth. Trisodium citrate and hydrazine hydrate were used as stabilizer and reductant respectively. Variations in four key parameters, namely, reductant ($N_2H_4.H_2O$) concentration, stabilizer concentration, temperature, and pH were done to alter the hydrogen bonding interaction.

Initially, $AgNO_3$ (1 mM, 10 ml) and citrate (80 mM, 0.5 ml) solution were mixed and hydrazine hydrate (2.5 mM, 2 ml) was added at pH 7 with constant stirring till a yellow colour appeared. In other synthesis sets, the hydrazine concentration was gradually increased in the following manner: 2.5→5.0→10→30→40 mM. Syntheses were also performed by changing the pH to 5 at room temperature (25 ^oC). Silver nanoparticles were also prepared lowering the temperature to 5 ^oC at pH 5 by varying the hydrazine concentration in a similar manner. Besides, such high concentrations, synthesis was also carried in the low concentration regime. Hydrazine concentration was reduced to 1.0 mM. At this sub-stoichiometric level of hydrazine (at 5 ^oC, pH 5), the time-span for the formation of nanocrystals increased to about 12 hours, which is in contrast to the time-span (15-30 mins.) in the high concentration regime. It should be noted that in all the abovementioned syntheses, pH of the solution was adjusted by dropwise addition of 1 M NaOH or 1 M H_2SO_4 solution.

2.3 Spectroscopic measurements:

All the samples were diluted twice and UV-Vis-near-IR absorption spectroscopy was performed on the Perkin Elmer Lambda 750 spectrophotometer. For FTIR spectroscopy, all the solution including citrate and citrate- hydrazine mixture were dried in vaccum dessicator overnight to obtained the powder sample. FTIR spectroscopy of the dried samples was carried out in the reflectance mode on the Shimadzu IR Prestige 21 spectrophotometer. The Raman spectroscopy was carried out on Renishaw InVia Raman Microscope.

2.4 Particle size and structural characterization:

The sample preparation for transmission electron microscopy (TEM) was done by putting a few drops of the as-prepared nanoparticles on the carbon coated copper grids (Ted Pella, product code: 01800) and immediate drying of the grids in vacuum desicator. TEM images were recorded on Zeiss microscope at an operating voltage of 200 kV to find the size, shape and structure of the NPs. Selected area electron diffraction (SAED) analysis was also done on the samples to determine the crystallinity.

2.5. SERS spectroscopy of arsenite anions:

Raman spectroscopy was first performed by the addition of aqueous As (III) ion solution (0.5 ppm) to the solution of both spherical (C_{hyd} = 2.5 mM, at pH 7 and 25 ^oC, SPR at 406 nm) and anisotropic silver nanocrystals (C_{hyd} = 40 mM, at pH 7 and 5 ^oC, SPR at 550 nm). Then the Raman spectra were again recorded by gradual addition of arsenite ion to the solution of anisotropic NCs (C_{hyd} = 40 mM, at pH 7 and 5 ^oC, SPR at 550 nm). The concentration of arsenite anion was increased in the following order: 0.5→1→1.5→2→2.5 ppm. Thus a calibration curve was made

3. Results and Discussion

3.1 Citrate-hydrazine H-bonding interaction and plasmon tunability

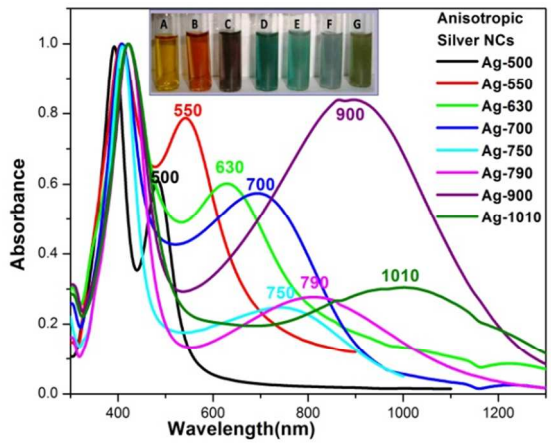

Figure 1. UV-Vis absorption spectra showing the plasmon peaks of the anisotropic silver NCs synthesized in a single step; Ag-500 (C_{hyd} = 40 mM, at pH 7 and 25 °C), Ag-550 (Chyd = 40 mM, at pH 7 & 5 °C), Ag-630 (C_{hyd} = 5 mM, at pH 5 & 5 °C), Ag-700 (C_{hyd} = 10 mM, at pH 5 & 5 °C), Ag-750 (C_{hyd} = 30 mM, at pH 5 & 5 °C), Ag-790 (C_{hyd} = 40 mM, at pH 5 & 5 °C), Ag-900 (C_{hyd} = 2.5 mM, at pH 5 & 5 °C), Ag-1010 (C_{hyd} =1.0 mM, at pH 5 & 5 °C). [Ag+]: [Cit^{3-}] ratio was kept constant at 1:4, [C_{hyd} : concentration of hydrazine hydrate]

We hypothesized that hydrogen bonding interaction between the stabilizer and reductant molecules, if properly harnessed, can direct the anisotropic growth of nanocrystals [Scheme 1]. Herein, we show that the combination of mild stabilizer and mild reductant, i.e, citrate and hydrazine hydrate, can yield silver nanocrystals with Vis-to-NIR tunable plasmon peaks [Figure 1] and tunable shapes [Figure 2]. As shown in Figure S1, addition of hydrazine in stoichiometric proportions at pH 7 and at room temperature (25 °C) gives a single peak at 400 nm, typical of spherical nanoparticles. In such a case, the citrate-hydrazine hydrogen bonding network breaks down as the reduction of Ag^+ ions proceeds. Therefore, our strategy was designed to keep hydrazine in excess so that the directional character of stabilizer-reductant hydrogen-bonded network is utilized for anisotropic crystal growth. The minimum amount of hydrazine to get a hint of such an effect was found to be 5 mM [Figure S1]. However, the effect gets more pronounced on increasing the reductant to an optimized concentration of 40 mM (at 25 °C, pH 7) which resulted in a distinct and intense second plasmon peak at 500 nm [Figure 1]. The peak further redshifts to 550 nm on decreasing the synthesis temperature to 5 °C (pH 7). The kinetics of reduction of Ag^+, nucleation and growth of nanocrystals is slowed down considerably at 5 °C. But, most importantly, the variation in the parameters was done so as to enhance the hydrogen bonding interaction between citrate and hydrazine. Low temperature retards the molecular motion and gives rigidity to the hydrogen bonding network. pH is another key parameter that affects the interaction through protonation or deprotonation of carboxyl and amine groups in citrate and hydrazine and which in turn may affect the pattern of crystal growth . Indeed, we found that at the lowered pH 5 (at 5 °C, C_{hyd}= 40 mM), the plasmon peak moves to790 nm in the near-IR region [Figure 1]. For the intermediate

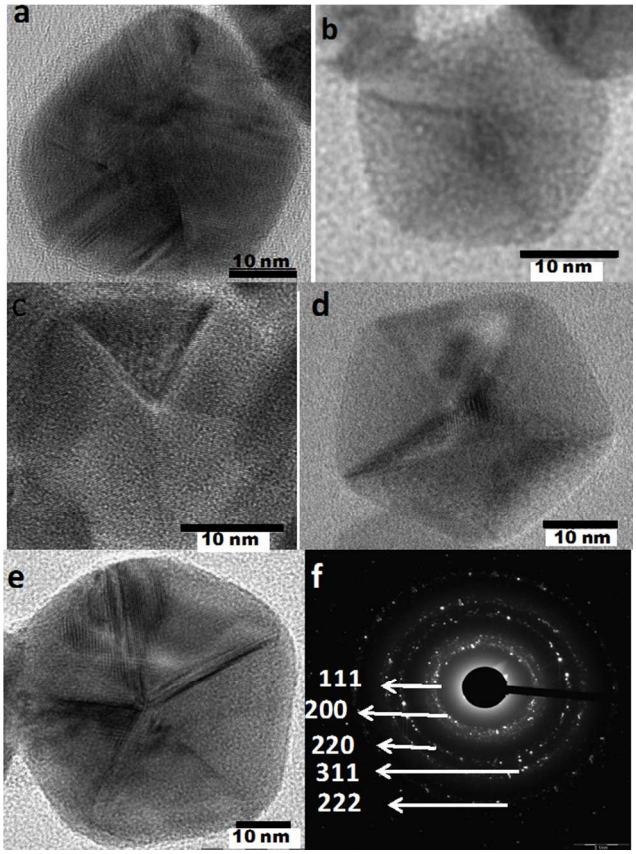

Figure 2. High resolution TEM images of anisotropic Ag NCs [scale bar :10 nm] (a) Ag-550, (b) Ag-790, (c) Ag-700, (d) Ag-900, (e) Ag-1010 and (f) SAED pattern showing the five bright rings corresponding to the 111, 200, 220, 311 and 222 hkl planes of fcc lattice of silver [JCPDS No. 04-0783].

concentrations of hydrazine (at 5 °C, pH 5), the plasmon peak is observed at 630 nm, 700 nm, 750 nm for 5mM, 10 mM and 30 mM respectively. Thus, the plasmon peak shows a gradual redshift (630→700→750→790 nm) with the increasing concentration of hydrazine (5→10→30→40 mM). Clearly, the role of excess hydrazine is quite evident in determining the plasmon peak position which arises due to anisotropic geometries adopted by the growing nanocrystals. The excess hydrazine can induce two things: 1. increase in reduction rate and 2. strengthening of the H-bonding network. The first one (reduction rate) hardly explains the tunability, it is the latter which guides the directional growth of the nanostructures.

All the single-step syntheses described above were carried out in a high concentration regime of hydrazine, 5-40mM, with molar ratio of [hydrazine]:[Ag^+] ranging from 1:1 to 8:1 that resulted in formation of nanocrystals within 15-30 minutes and plasmonic tunability from 500 nm to 790 nm was achieved. If the hydrazine concentration is increased beyond 40 mM, no further redshift is observed. Surprisingly, the greatest redshift is achieved on performing the synthesis in the low concentration regime that includes sub-stoichiometric level of hydrazine at 5 °C and at pH 5. Under these conditions, upon prolonged stirring for 12 hours, plasmon peak moves to 900 nm and 1010 nm respectively for 2.5 mM and 1.0 mM hydrazine [Figure 1]. It is evident that the

reduction rate becomes extremely slow in such cases. In the initial stages of synthesis, the fraction of hydrazine molecules undergoing the reaction is minuscule. Therefore, most of the hydrogen bonding network remains intact as the nucleation occurs and the growing nanocrystals acquire the shape and structure according to the constraints put up by the citrate-hydrazine matrix.

Interesting pattern emerges on carrying out structural analysis of the tunable plasmonic nanocrystals by Transmission Electron Microscopy (TEM). Figure 2 shows the HRTEM images in which anisotropic shapes of the nanocrystals are clearly visible. The sample Ag-550 has a pentagonal plate like structure having three sides of 25 nm each while two of them is 15 nm each. The change in synthesis pH has profound influence on the shape and size of NCs. With a change in synthesis pH from 7 to 5 and for the same hydrazine concentration of 40 mM, the pentagonal nanoplates transform into nanopyramids with an equilateral pentagonal base having an edge length of 18 nm (sample Ag-790). The evolution of shapes, from nanoplates to nanopyramids, with change in pH from 7 to 5 is attributed to change in hydrogen bonding pattern due to partial protonation of citrate. On decreasing the concentration to 10 mM, the shape remains the same, pentagonal pyramidal, but the edge length decrease to 15 nm (Ag-700). However, in the low concentration regime (less than 5 mM), an entirely contrasting result is obtained. As the concentration of hydrazine is reduced from 2.5 mM to 1.0 mM, the nanopyramids become bigger (edge length, 22 nm→ 30 nm) and the plasmon peak shows a huge redshift (900 nm→1010 nm). This clearly indicates that there two different mechanisms of crystal growth for the low and high concentration regimes. Considering the energies of different faces of an fcc silver crystal ($\sigma_{111} < \sigma_{100} < \sigma_{110}$)[2b,c], the growth is likely to be promoted along the {111} and {100} planes to minimize the surface energy. The HRTEM images of the NCs in the high concentration regime suggest that the particles predominantly grow along {111} plane [Figure S2]. However, in the low concentration regime (including sub-stoichiometric level), the growth occurs along {100} plane [Figure S2]. The statistical analysis of TEM images is shown in Figure S3 which indicates narrow size distribution. A closer examination of the NCs formed at sub-stoichiometric level reveals multiple twinned structures in the lattice [Figure S2]. At such low pH, low temperature and ultra-low concentration of hydrazine, the rate of reduction and crystal growth becomes extremely slow leading to twinings. Similar observations were also made by Xia and co-workers[2c] while working on polyol synthesis of such nanostructures.

3.2 Second derivative FTIR analysis of citrate-hydrazine H-bonding interactions

Underlying all these interesting variation in nanocrystal geometry and plasmonic properties is the shape directing ability of hydrogen bonding network formed due to interaction of citrate and hydrazine molecules. To understand these interactions of capping and reducing agent, FTIR spectroscopy was done at pH 5 and 7 for different concentrations of hydrazine and citrate. The complete FTIR spectra covering the range 400-4000 cm^{-1} is shown in Fig S4(a,b). However, the most significant changes

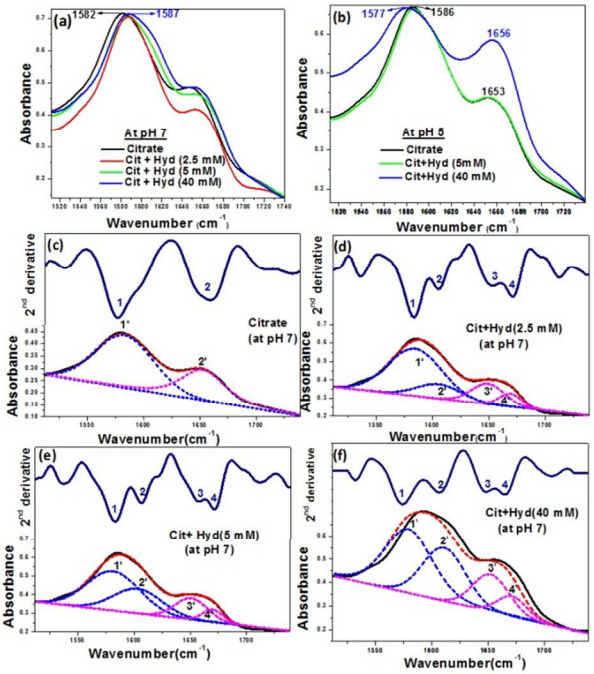

Figure 3. FTIR spectra in 1512-1739 cm^{-1} region of pure citrate and citrate mixed with different concentrations of hydrazine at pH 7(a) and pH 5 (b). Second derivative spectra and deconvolutions of FTIR peaks at pH 7 of pure citrate (c) and citrate mixed with varying concentrations of hydrazine: (d) 2.5 mM, (e) 5 mM and (f) 40 mM . (— raw FTIR data,····· and····· deconvoluted peaks, ····· overall fitting, — second derivative plot) {Band assignments of deconvolutions: 1,1'- free -COO- asymmetric stretch ; 2,2'- H-bonded -COO- asymmetric stretch ; 3,3' noncoordinated H_2O deformation; 4,4' coordinated H_2O deformation.}

were observed in the spectral region of 1500-1750 cm^{-1} which is shown in [Fig.3(a,b)]. At pH 7, the COO- asymmetric stretch appears at 1579 cm^{-1} for citrate which blueshifts by 8 cm^{-1} on addition of 2.5 mM hydrazine. Further addition of hydrazine does not cause a change in the peak position, however, a gradual broadening of the peaks is observed. As the hydrazine concentration is increased, 2.5 → 5.0→40 mM, the FWHM of the peak also increases in the following manner, 46 →51→55 cm^{-1}. The broadening could be well attributed to increased hydrogen bonding interaction between citrate and hydrazine. At pH 5, the citrate COO- asymmetric stretch appears at 1586 cm^{-1}, which shows a 9 cm^{-1} redshift on addition of 40 mM hydrazine [Fig 3b]. On considering the acid dissociation constants for hydrazine ($pKa=8.1$)[16a] and citrate ($pKa_1=3.09$, $pKa_2=4.79$, $pKa_3=5.41$),[16b] it is clear that one of the three carboxylate anionic groups also gets protonated as the pH is reduced from 7 to 5. Thus, in native citrate also, pH dependent shift is observed. This drastically affects the hydrogen bonding pattern, which is reflected in the FTIR spectra. The proof of hydrogen bonding is also seen in the Raman spectra (Figure S5) in which a new peak appears at 1607cm^{-1} for citrate-hydrazine (C_{hyd}=40mM) mixture.

To gain further insights into the hydrazine-citrate hydrogen bonding interactions, rigorous second derivative analysis was performed on FTIR spectra and the peaks were deconvoluted into several Gaussian functions. Overlapping peaks in the raw data can be resolved in the second derivative spectra and finer details can be obtained.[17] As shown in Fig 3d-f , two new peaks appear

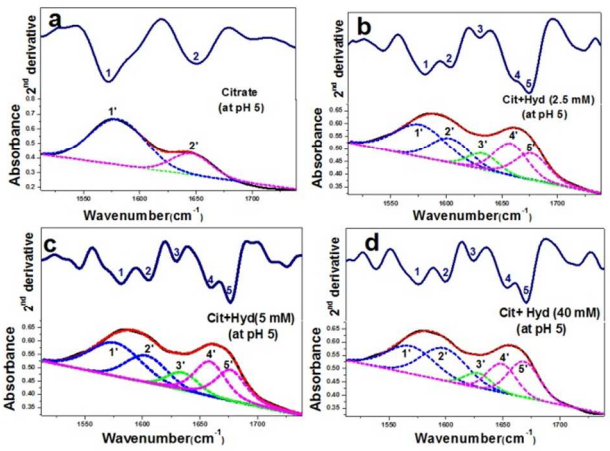

Figure 4. Deconvolutions of FTIR spectra of pure citrate (a), citrate mixed with 2.5 mM N_2H_4(b), 5 mM N_2H_4 (c) and 40 mM hydrazine (d) in the 1512-1739 cm^{-1}region. (— raw FTIR data,····· and····· deconvoluted peaks, ····· overall fitting, — second derivative plot) {Band assignments of deconvolutions: 1,1'- free -COO^- asymmetric stretch ; 2,2'- H-bonded -COO^- asymmetric stretch ; 3,3' 4,4' noncoordinated H_2O deformation band ; 4,4' coordinated H_2O deformation band.

on hydrazine addition to citrate at pH 7, which were not initially present in the FTIR spectra of either citrate or hydrazine alone. It clearly indicates that these peaks originate from the citrate and hydrazine interaction. The peak appearing at 1605 cm^{-1} can be ascribed to the vibrations of COO^- hydrogen bonded to hydrazine (H-bonded COO^-). Similarly, the peak for deformation mode of water appearing at 1660 cm^{-1} in pure citrate splits into two peaks on addition of hydrazine. We further note that the relative intensity of the 2,2' deconvolution i.e., H-bonded COO^-, gradually increases. On going from hydrazine concentration of 2.5→5.0→40 mM, the intensity ratio of the peaks (2, 2')/ (1,1') increases in the following order, 0.24→0.50→0.81. It implies that initially when the hydrazine concentration is doubled from 2.5 to 5 mM, the intensity of H-bonded COO^- peak is also doubled. Further eight fold increase in the concentration causes the FTIR intensity ratio to rise by 60% only. The enhanced hydrogen bonding between reductant and stabilizer affects the nucleation and growth kinetics which results in evolution of anisotropic shapes and plasmonic properties. As shown in Fig. S1, a single plasmon peak at 405 nm is observed for 2.5 mM hydrazine. On doubling the concentration, a second plasmon peak appears at 489 nm which is rather broad with FWHM of 134 nm. As the concentration is further raised to 40 mM, the position of the second plasmon peak remains nearly the same. However, the relative intensity of the peak increases and its FWHM substantially reduced to 63 nm. The change in plasmonic properties corresponds to change in shape from nanospheres (C_{Hyd} = 2.5 mM) to pentagonal nanoplates (C_{Hyd} = 40 mM).

At pH 5, the pattern of citrate-hydrazine hydrogen bonding is substantially altered due to protonation of one of the carboxylate groups. The second derivative FTIR analysis (1550-1750 cm^{-1}) reveals two additional peaks for the citrate-hydrazine solution [Figure 4]. The peak 2,2' appearing at 1605 cm^{-1} attributed to H-bonded COO^- shows a rise in the relative intensity [ratio of peaks (2,2')/(1,1')] from 0.42 to 0.88 as the concentration of hydrazine is raised gradually from 5 mM to 40 mM. The hydrogen bonding interactions at pH 5 lead to versatile tunablity of plasmon peaks from visible (630 nm) to near-IR (790 nm) region. As can be seen in Figure 5, a linear correlation has been obtained between the plasmon peak position and the relative intensity of H-bonded COO- peaks. This clearly establishes the link between H-bonding interaction and plasmon tunability at pH 5. This is in contrast to the citrate-hydrazine behaviour at pH 7, in which no change in plasmon peak position was observed with the enhanced hydrogen-bonding interactions.

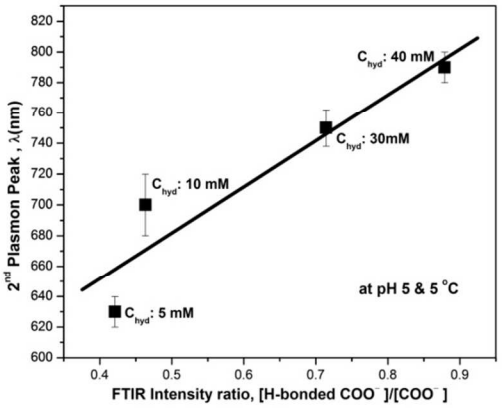

Figure 5. Variation of plasmon peak position with change in relative intensity of H-bonded COO- FTIR absorption peaks. [each datapoint is a mean of three measurements].

3.3 Temporal evolution of near-IR plasmonic nanocrystals

Since the time of addition of reagents to the formation of silver nanocrystals, the temporal evolution of plasmonic properties was followed spectroscopically. At different time intervals, aliquots were taken and UV-Vis absorption spectra was recorded. In the initial phases of growth, after 5 minutes, two peaks appear in the visible region at 406 nm and at 501 nm (Fig. 6a). It suggests that the inception of structural anisotropy in the nanocrystals occurs during the nucleation stage. With the passage of time, the anisotropic nanocrystal grows bigger, and the second plasmon peak gradually shows a red-shift. After 20 minutes of crystal growth it moves to the near-IR spectral region at 696 nm and finally after 30 minutes the plasmon peak further shifts to 809 nm. Beyond this point, no change in plasmonic properties is observed indicating the completion of growth process. The plasmonic redshift follows a linear pattern with time as shown in the inset. All these while the plasmon intensity of both peaks keeps increasing. However, the ratio of integrated plasmon intensities (area under the peak, A_{SPR2}/A_{SPR1}) of the two peaks shows an abrupt rise from 0.6 (at 5 min.) to 2.1 (at 10 min) initially. Subsequently, the ratio decreases linearly and reaches unity after 30 minutes. For these calculations, the absorption spectra were deconvoluted, fitted with two Gaussian-like functions and then area under the each peak was taken which is shown in Figure S6 and Table S2. The width (FWHM) of the plasmon peaks also shows interesting variation as shown in the inset of Figure 6b. The FWHM of the first SPR peak doesnot

undergo much change. However, the FWHM of the second peak increases linearly concomitant with the red-shift of the peak position. After 5 minutes of growth, the FWHM is 77 nm which increases to 352 nm at the completion of nanocrystal growth.

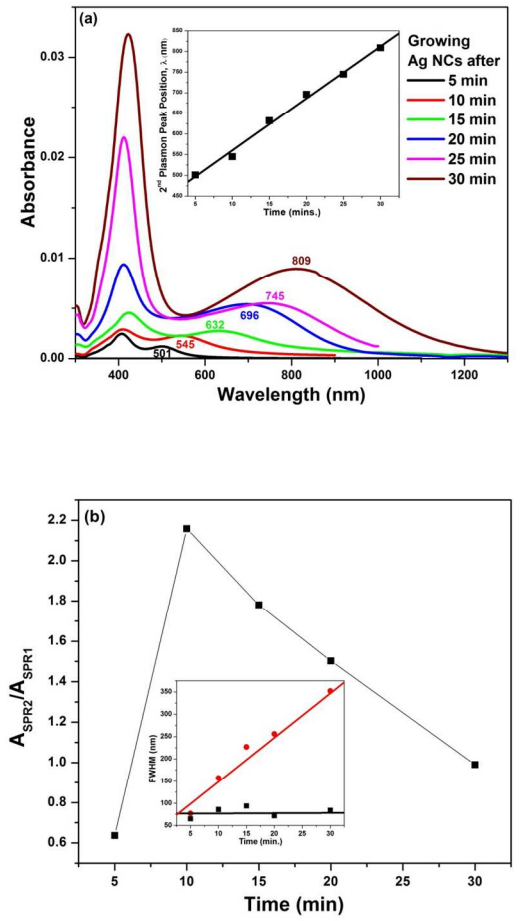

Figure 6. Temporal evolution of plasmonic properties of anisotropic silver NCs at pH 5 and 5 °C. (a) UV-Vis absorption spectra taken at different time intervals during the growth, inset: variation in 2nd plasmon peak position with time; (b) Ratio of plasmon intensities (A_{SPR2}/A_{SPR1}) as a function of time, inset: change in FWHM of each peak during growth, ■- SPR1, ●- SPR2 [Integrated plasmon intensity was taken as the area under the deconvoluted peaks as shown in Fig S5]

3.3 Surface-enhanced Raman scattering

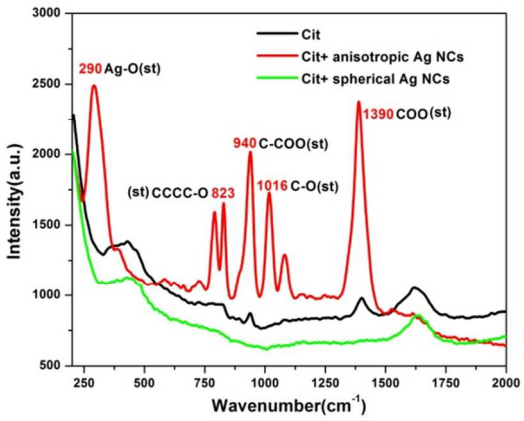

Figure 7. Enhancement of Raman peaks of citrate on the surface of anisotropic Ag NCs. (non-resonant condition: laser wavelength = 633 nm, plasmon wavelength =550 nm)

To realize the potential of these anisotropic silver NCs in surface-enhanced Raman spectroscopy (SERS),[18] experiments were performed in non-resonant conditions using 633-nm laser. The capping agent, citrate, exhibited notable enhancement of Raman signals on the surface of anisotropic NCs, Ag-550 [Figure 7]. The result bears significance as citrate is not known to be a Raman reporter and its only SERS spectrum by previous workers[19] was obtained under resonant conditions. In contrast to anisotropic NCs, we found no SERS enhancement for spherical NCs in non-resonant conditions. The maximum enhancement has been observed in case of asymmetric stretching of –COO group at 1390 cm^{-1}. Several peaks which were invisible in pure citrate get enhanced such as the stretch modes of C-O, C-COO and CCCC-O at 1016, 940 and 828 cm^{-1} respectively.[20]

3.5 SERS detection of As (III) species

Encouraged by the results with citrate, we also explored the possibility of detection of an inorganic contaminant, arsenite, present in ground water through solution phase SERS spectroscopy. The Raman intensity of stretch mode of arsenite (As(III)-O stretch) at 721 cm^{-1} was enhanced in the presence of the anisotropic NCs (Ag-550) than spherical NCs even at an ultralow concentration of 0.28 ppm (Figure 8a). Further, as the concentration of As (III) is increased, the Raman intensity increases gradually. The SERS signal and As (III) concentration show a good linear relationship as in Figure 8b. This plot of Raman intensity vs As (III) concentration can act as a calibration curve using which unknown As (III) in a test- sample can be determined. The limit of detection was found to be 0.15 ppm.

This is a simplified approach as colloidal nanoparticles can be directly used for SERS-based detection of inorganic contaminants in a non-resonant condition. In contrast, most of the previous reports[21] necessarily involve 2-D assembly and making a nano-thin film for SERS spectroscopy of arsenite anions. Recently, Li et al[22] reported As^{3+}-induced aggregation of colloidal silver nanocrystals and subsequent enhancement of SERS signal of the capping agent , mercaptopyridine, was used to indirectly detect trace amount of As^{3+}. In contrast, we directly measure the enhancement of SERS signals of As^{3+}-O vibrations

on the surface of non-aggregated silver nanocrystals and the As^{3+} is detected without using Raman reporter molecules. Thus, the findings of this work will have strong implications in developing simple but efficient SERS based sensors for inorganic contaminants.

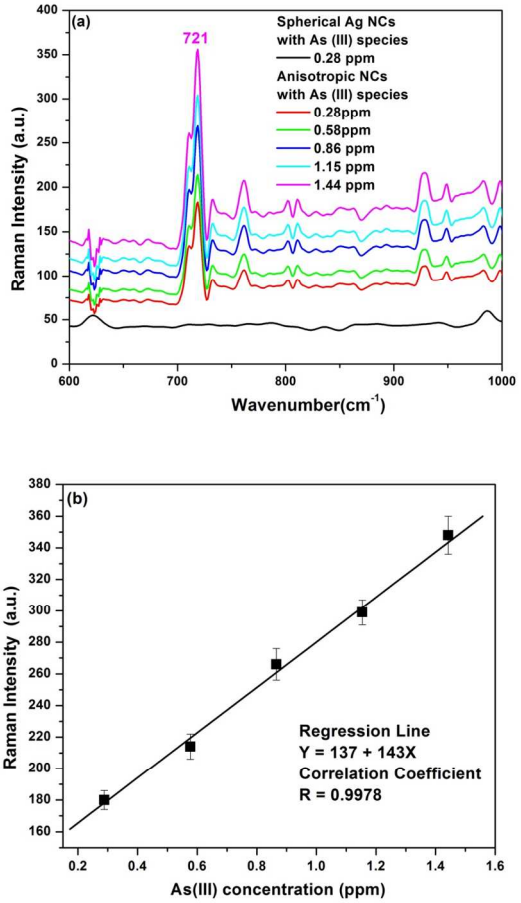

Figure 8. (a) SERS spectra of As(III)-O vibrations for varying As(III) concentration on spherical as well as anisotropic Ag NCs (Note: No enhancement is observed for spherical NCs.) (b) Linear relationship between SERS signal and As(III) concentration. [each datapoint is a mean of three measurements] (non-resonant condition: laser wavelength = 633 nm, plasmon wavelength =550 nm)

4. Conclusions

In conclusion, a simplified direct synthesis route to anisotropic silver nanocrystals has been developed. Hydrogen bonding interactions between stabilizer and reductant, citrate and hydrazine, has been established as a chief architect of nanocrystal characteristics. We clearly show that the shape, size and plasmonic properties can be effectively altered by tailoring these hydrogen bonding interactions and by making use of its directional character. The shapes undergo tremendous variation from nanospheres to nanoplates to nanopyrmaids and concomitantly, the plasmon peak has been tuned from visible (500 nm) to near-IR (1010 nm) region. All of these have been achieved in a single shot addition of reagents at less than ambient temperature; that underscores the simplicity of the method in comparison to the existing ones. Thus, the work opens up new avenues to obtain other plasmonic nanomaterials with greater ease. We also show a unique behavior, Raman enhancement as well as Raman quenching, of the citrate molecules on the surface of these anisotropic silver nanocrystals. These nanocrystals also cause huge SERS enhancement for arsenite anions, a common contaminant present in groundwater. Based on this behaviour, a non-resonant SERS spectroscopic method has been developed for detecton of As(III) species.

Acknowledgements

AP gratefully acknowledges the financial support from DST, Govt. of India (grant no. SR/NM/NS-1047/2012 and SB/FT/CS-84/2011). AS thanks DST, Govt of India for KVPY fellowship. One of the authors (S. P.) is thankful to Birla Institute of Technology, Mesra for the award of the institute's fellowship. The authors thank all the staff of CIF and Dr. Rishi Sharma, Dept. of Physics, BIT Mesra for their cooperation in various instrumental measurements.

Notes and references

[a]*Department of Applied Chemistry, Birla Institute of Technology, Mesra, Ranchi-835215, India*
[b]*Indian Institute of Science Education and Research, Pune, India*
[c]*Department of Chemistry, Central University of Bihar, Gaya- 823001, India*
[d]*UGC-DAE Consortium for Scientific Research, Kalpakkam Node, Kokilamedu-603104, India*
[#]*previously at: Department of Applied Chemistry, Birla Institute of Technology, Mesra, Ranchi-835215, India*
**Corresponding author, email: apriyam@cub.ac.in; Phone: +91-8521147173, Fax: +91-631-2222124*

† Electronic Supplementary Information (ESI) available: [temperature optimization; EDX spectra of HAgNS; TEM, SAED and DLS of Ag_2O NPs; FTIR spectra of GSH-HAgNS, pH dependent aborption spectra of HAgNS]. See DOI: 10.1039/b000000x/

Supporting Information: TEM & HRTEM images, FTIR and Raman spectra of citrate and hydrazine. This material is available free of charge via the Internet at http://pubs.acs.org.

1. (a) J. Watt, S. Cheong and R.D. Tiley, *Nano Today,* 2013**, 8**, 198-215 (b) M.H. Huang and P.-H. Lin, *Adv. Funct. Mater.* 2012, **22**, 14–24 (c) S. Trudel, *Gold Bulletin*, 2011, **44**, 3-13 (d) K. Zhou and Y. Li, *Angew. Chem. Int. Ed.*, 2012, **51**, 602-613
2. (a) M. Rycenga, C. M. Cobley, J. Zeng, W. Li, C. H. Moran, Q. Zhang, D. Qin and Y. Xia, *Chem. Rev*. 2011, **111**, 3669–3712. (b) P. Yu, J. Huang and J. Tang, *Nanoscale Res Lett*. 2011**, 6**, 467 (c) Y. Xiong, A. R. Siekkinen, J. Wang, Y. Yin, M. J. Kim and Y. Xia, *J. Mater. Chem*. 2007, **17**, 2600–2602 (d) B. Wiley, T. Herricks, Y. Sun and Y. Xia, *Nano Lett.*, 2004, **4**, 1733-1739
3. (a) L. Tong, Q. Wei and A. Wei and J.X. Cheng, *Photochem. Photobiol*. 2009, **85**, 21–32, (b) K-T. Yong, M. T. Swihart, H. Ding, and P. N. Prasad, *Plasmonics,* 2009, **4**, 79–93.
4. J. C. Andrew and L.W. Jennifer, *J. Am. Chem. Soc.*, 2012, **2**, 37-54.
5. (a) S. Lal, N. K. Grady, J. Kundu, C. S. Levin, J. B. Lassiter and N. J. Halas, *Chem. Soc. Rev*. 2008, **37**, 898-911. (b) R. A. Tripp, R. A. Dluhy and A. Zhao. *Nano Today*, 2008, **3**, 3-4.

6.(a) H. A. Atwater and A. Polman, *Nat. Mater*, 2010, **9**, 205-213. (b) S. Pillai and M. Green, *Sol. Energy Mater. Sol. Cells* 2010, **94**, 1481-1486.

7. S. Guo and E. Wang, *Nano Today*. 2011, **6**, 240-264.

8. (a) A. Corma and H. Garcia, *Chem. Soc. Rev*. 2008, **37**, 2096–2126. (b) S. Bastide, N. L. Quang, R. Monna and C. Lévy-Clément, *Phys. Status Solidi* 2009, **6**, 1536–1540.

9. (a) S. Link and M. El Sayed, *J. Phys. Chem. B* 1999**, 103**, 4212-4217. (b) X. Huang and El Sayed, *J. Adv.Res.* 2010, **1**, 13-28.

10. (a) M. Li, S. Johnson, H. Guo, E. Dujardin and S. Mann, *Adv. Funct. Mater*. 2011, **21**, 851-859. (b) I. Blakey, Z. Merican and K. J. Thurecht, *Langmuir* 2013, **29**, 8266−8274. (c) P. Dey, S. Zhu, K.J. Thurecht, P. M. Fredericks and I. Blakey, *J. Mater. Chem. B*, 2014, **2**, 2827–2837. (d) T. Kim, K. Lee, M.-S. Gong, and S.-W. Joo, *Langmuir* 2005**, 21**, 9524-9528.

11. J. Zhang, M. R. Langille and C. A. Mirkin, *Nano Lett*., 2011. **11**, 2495–2498.

12. B.J. Wiley, Y. Chen, J. M. McLellan, Y. Xiong, Z-Y. Li, D. Ginger and Y. Xia, *Nano Lett.*, 2007, **7**, 1032-1036.

13. P. C. Angelome, H. H. Mezerji, B. Goris, I. Pastoriza-Santos, J. Pérez-Juste, S. Bals and L. M. Liz-Marzán, *Chem. Mater*. 2012, **24**, 1393−1399.

14. (a) Q. Huang and X. Zhu, *Talanta*, 2013, **105**, 117-123. (b) T. Deckert-Gaudig, F. Erver and V. Decker, *Langmuir* 2009, **25**, 6032–6034

15. (a) S. Ghader, M. Manteghian, M. Kokabi and R. S. Mamoory *Polish J. Chem.,* 2007, **81**, 1555–1565. (b) Z. Cao, H. Fu, L. Kang, L. Huang, T. Zhai, Y. Ma and J. Yao, *J. Mater. Chem.*, 2008, **18**, 2673–2678

16. (a) M. Mazloum-Ardakani et al, *Turk J. Chem*, 2010 , **34**, 229–240. (b) Dawson, R.M.C., Data for Biochemical Research, Clarendon Press, Oxford, 1969, pp. 481.

17. A. Priyam, D.E. Blumling and K.L. Knappenberger, Jr., *Langmuir*, 2010, **26**, 10636-10644.

18. (a) Y. Li, N. Koshizaki, H.Wang, and Y. Shimizu, *ACS Nano*, 2011, **5**, 9403–9412. (b) J. Hazard. Mater. 2013, **248–249**, 435–441**.**

19. O. Sliman, L.A. Bumm, R. Callaghan, C. O. Blatchford, and M. Kerker, *J. Phys. Chem*. 1983, **87**, 1014-1023

20. C. H. Munro, W. E. Smith, M. Garner, J. Clarkson and P. C. White, *Langmuir*, 1995, **11**, 3712-3720.

21. (a) M. Mulvihill, A. Tao , K. Benjauthrit, J. Arnold and P. Yang,, *Angew. Chem. Int. Ed*., 2008, **120**, 6556–6560. (b) Z. Xua, J. Haoa, F. Lib and X. Meng, *J. Colloid Interface Sci*., 2010, **347**, 90-95.

22. J. Li, L. Chen, T. Lou and Y. Wang, *ACS Appl. Mater. & Interfaces*, 2011, **3**, 3936-3941.

Citrate-hydrazine hydrogen-bonding driven single-step synthesis of tunable near-IR plasmonic, anisotropic silver nanocrystals: Implications in SERS spectroscopy of inorganic oxoanions

Sataruapa Pattanayak,[a] Abhishek Swarnkar,[b] Amiya Priyam,[c,#,*] and Gopal M. Bhalerao[d]

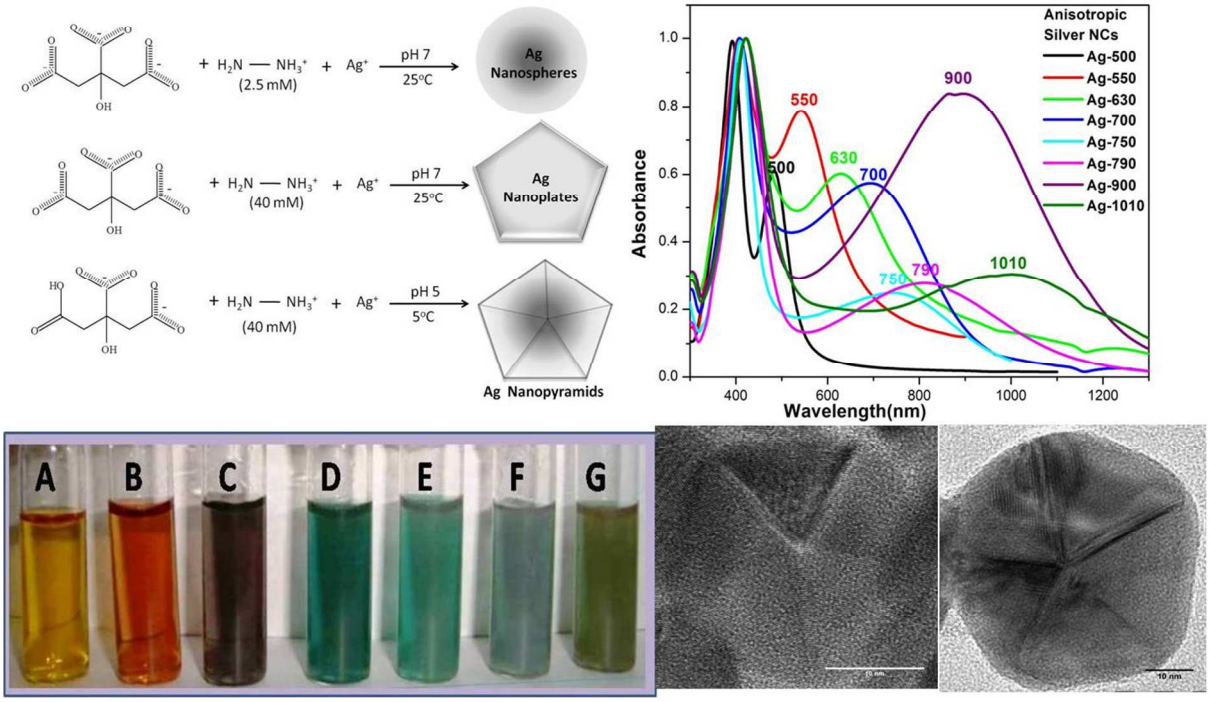

Anisotropic silver nanocrystals (NCs) having Vis-to-NIR plasmon tunability has been synthesized by tailoring the hydrogen-bonding interactions between a mild stabilizer (citrate) and mild reductant (hydrazine hydrate).